Planetary Nebulae: A Universal Toolbox in the Era of Precision Astrophysics
Proceedings IAU Symposium No. 384, 2025
O. De Marco, A. Zijlstra & R. Szczerba, eds.
doi:10.1017/S1743921324000462

The structure of emission lines in planetary nebulae at very high spectral resolution†

Michael G. Richer[1], José Alberto López[1], Anabel Arrieta[2], Lorena Arias[2] and Silvia Torres-Peimbert[3]

[1]Instituto de Astronomía, Universidad Nacional Autónomo de México, Apartado Postal 106, CP 22800 Ensenada, Baja California, México

[2]Departamento de Física y Matemáticas, Universidad Iberoamericana, Prolongación Paseo de la Reforma 880, Lomas de Santa Fe, CP 01210, Ciudad de México, México

[3]Instituto de Astronomía, Universidad Nacional Autónomo de México, Apartado Postal 70-264, CP 04510 Ciudad de México, México

Abstract. We present spectroscopy of NGC 3242, NGC 6153, and NGC 7009 at very high spectral resolution ($\lambda/\delta\lambda = 75,000 - 100,000$) obtained with the Manchester Echelle Spectrograph at the 2.1m telescope of the Observatorio Astronómico Nacional on the Sierra San Pedro Mártir. We study the kinematics of the plasma within the nebular shells, decomposing the observed line profiles considering the microscopic, macroscopic, and observational processes that broaden them. The residual kinematic structure, defined as the sum of velocity gradients, kinematic structure, and seeing dominates the broadening of the lines of heavy elements. We estimate the effect of velocity gradients, finding that it can account only for a minority of this residual kinematic structure. Whatever the origin of this residual kinematic structure, it is an important component of the kinematics of the ionized plasma within the nebular shell and implies an important energy source that is not contemplated in photoionization models of planetary nebulae.

Keywords. planetary nebulae, spectroscopy, kinematics, turbulence

1. Introduction

We present preliminary results of observations of the planetary nebulae NGC 3242, NGC 6153, and NGC 7009 at very high spectral resolution. Our objective is to study the structure of the plasma within the nebular shell, as illustrated in Figure 1. In contrast to traditional studies of the internal kinematics of planetary nebulae, where the focus is usually on studying the expansion of the nebular shell as a function of the ions observed, here we study the motions within the nebular shell itself. To do so, we must separate the effects of microscopic physical processes from the physical processes that operate on macroscopic scales. We mostly follow the precepts laid out in Sabbadin et al. (2008).

A variety of processes contribute to broaden the emission line profile arising from a plasma. We may quantify several of these effects. First, each line has a natural line width due to the lifetime of the line's upper level. For the permitted lines we consider, the width is of order m/s in velocity space (Gaussian σ; e.g., Pradhan & Nahar 2011). For the much longer lifetimes of the forbidden lines, the width is orders of magnitud smaller than this. We ignore this natural line width because it is much less than the effects that follow. Second, the H and He lines have components whose spacing is less than the thermal broadening, and so are not resolved even when the instrumental resolution would allow

† MGR and JAL acknowledge funding from DGAPA-UNAM grants IG101233 and IN111124.

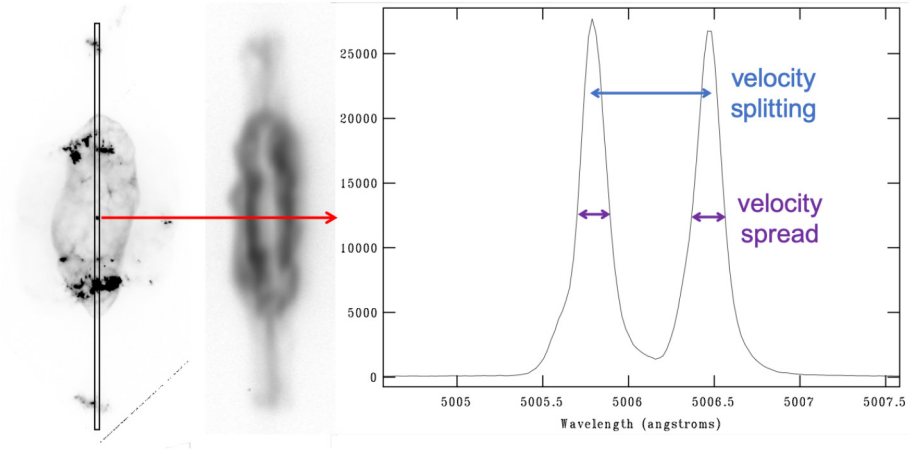

Figure 1. This figure illustrates our experiment. The left panel sketches our slit over the HST image of NGC 7009 ([N II] λ6584; Prop. ID 11122, PI Balick). The middle panel presents the resulting two dimensional spectrum, the position-velocity (PV) diagram. The approaching (left) and receding (right) sides of the nebular shell are clearly distinguished due to their differing Doppler shifts. The ellipse in the PV diagram, due to the main shell, closes at the top and bottom because the velocity is perpendicular to the line of sight at those positions. The right panel presents a spatial cut of the PV diagram at the position of the central star (the position of the arrow) from the [O III] λ5007 spectrum. The two peaks represent the emission from the approaching and receding sides of the shell, separated by their velocity splitting. What interests us here is the widths of these emission peaks (FWHM), the velocity spread, and the physical processes responsible for these widths.

it. This broadening has a typical width of 5 km/s, but will depend upon the particular lines (e.g., Clegg et al. 1999). Third, the thermal motions of the ions in the plasma imply a broadening, $\sigma_{th} = \sqrt{83.1(T_e/10^4/A)}$ km/s (e.g., Lang 1980), where T_e is the electron temperature (in K) and A the atomic mass of the ion involved (in atomic mass units), i.e., $\sigma_{th} = 9.1$ km/s for H and 2.3 km/s for O at 10^4 K. Fourth, the instrumental point spread function will broaden the line profile by $1.3 - 5.4$ km/s for spectral resolutions between 10^5 and 20,000 respectively.

There are other broadening mechanisms, whose effect upon the observed line width are much less clearly defined. There may be both organized and disorganized motions within the nebular shell. Apart from the expansion of the nebular shell, it is well-known that the velocity splitting observed between the approaching and receding sides varies as a function of the ionization potential of the ions involved (Wilson 1950), i.e., there is often a velocity gradient from the inner to the outer edge of the nebular shell. Both the expansion of the nebular shell and the velocity gradient are ordered motions, but there may also be macroscopic turbulence, due to large-scale, disordered motions within the plasma. In what follows, we will refer to the sum of these macroscopic effects as the nebular shell's "kinematic structure".

Finally, the spatial resolution of the observations is finite. So, if nearby lines of sight have different kinematics and if these lines of sight cannot be spatially resolved, they will contaminate and broaden the emission profile along any given line of sight. Our experiments indicate that this effect is probably not important for scales of $1'' - 2''$ in our objects, whose sizes are of order $30''$.

https://doi.org/10.1017/S1743921324000462 Published online by Cambridge University Press

2. Observations

The observations were undertaken at the Observatorio Astronómico Nacional on the Sierra San Pedro Mártir (OAN-SPM), Baja California, México using the Manchester Echelle Spectrograph (MES; Meaburn et al. 2003) installed on the Cassegrain focus of the 2.1m telescope. The MES is a long-slit, echelle spectrograph that uses narrow-band filters to isolate the spectral order of interest. The spectral resolution is set by the width of the entrance slit. For the observations used here, a 39 μm slit was used, yielding a maximum spectral resolution ($\lambda/\delta\lambda$) of order 10^5 at the C II λ6578 line. The observations were obtained in various observing runs beginning with the first trial observations in 2018 and continuing to June 2023. We obtained spectra with filters that allowed observing the following emission lines: O II $\lambda\lambda$4639,4649,4662, N III $\lambda\lambda$4634,4641, He II $\lambda\lambda$4686,6560, [O III] λ5007, He I λ5016, [N II] $\lambda\lambda$6548,6563, Hα, and C II λ6578. Here, we present observations of NGC 3242, NGC 6153, and NGC 7009, but we also have similar spectra for IC 418, NGC 6543, NGC 6572, NGC 6826, and NGC 7027.

The reduction of these spectra followed the standard practice for long-slit spectroscopy (e.g., Massey et al. 1992) and is described in Richer et al. (2017). When necessary, cosmic rays were edited out of the object spectra. The overscan area of the images was then averaged and subtracted for all images. Mean, overscan-subtracted bias images were used to create two-dimensional bias patterns and subtracted from all other images. In some cases, flat field images were obtained of the internal tungsten lamp and used to create flat field images that were then applied to the object spectra. We did not calibrate in flux.

We also consider observations of NGC 6153 obtained on 2002 June 8 at the European Southern Observatory (ESO) using the Ultraviolet and Visual Echelle Spectrograph (UVES; Dekker et al. 2000) mounted on the Very Large Telescope (VLT) Kuyen (UT2) and retrieved from the ESO archives (program 69.D-0174A, PI Danziger). These spectra include the entire optical range at a spectral resolution of approximately 30,000 and have been described in detail elsewhere (Richer et al. 2022).

3. Analysis and Results

For the MES spectra, we measure the velocity spread (Figure 1) of two sides of the nebular shell along the line of sight to the central star (NGC 3242, NGC 6153, and NGC 7009), what Sabbadin et al. (2008) refer to as the "central star pixel line". We consider a spatial extent of 1″ for the analysis. We measure the FWHM of the emission peaks, fitting a Gaussian function, or several if the line can be reliably decomposed into several components. In all cases, one component strongly dominates the emission profile and we present results only for that component. As the spectrum in Figure 1 illustrates, the profiles may be complex within the main shell, but usually one emission component dominates along any given line of sight.

We decompose the width of this dominant component assuming that the line fine structure, the thermal broadening, and the instrumental point spread function are all Gaussian in form. Hence, we compute the residual kinematic structure, ΔW_{ks} as

$$\Delta W_{ks}^2 = FWHM_{obs}^2 - FWHM_{fs}^2 - FWHM_{th}^2 - FWHM_{psf}^2$$

where $FWHM_{obs}$, $FWHM_{fs}$, $FWHM_{th}$, and $FWHM_{psf}$ are the observed width, the fine structure broadening, the thermal width, and the instrumental broadening, all as $FWHM = 2.355\sigma$. The only lines affected by fine structure are Hα and He II $\lambda\lambda$4686,6560. For Hα, we adopt $FWHM_{fs} = 7.5$ km/s based upon García-Díaz et al. (2008). We are working on estimates for the He II lines (see also Sabbadin et al. 2008). For the thermal broadening, we currently assume $T_e = 9,000$ K, though this may be an over-estimate for the C II and O II lines in these objects. For the instrumental broadening,

https://doi.org/10.1017/S1743921324000462 Published online by Cambridge University Press

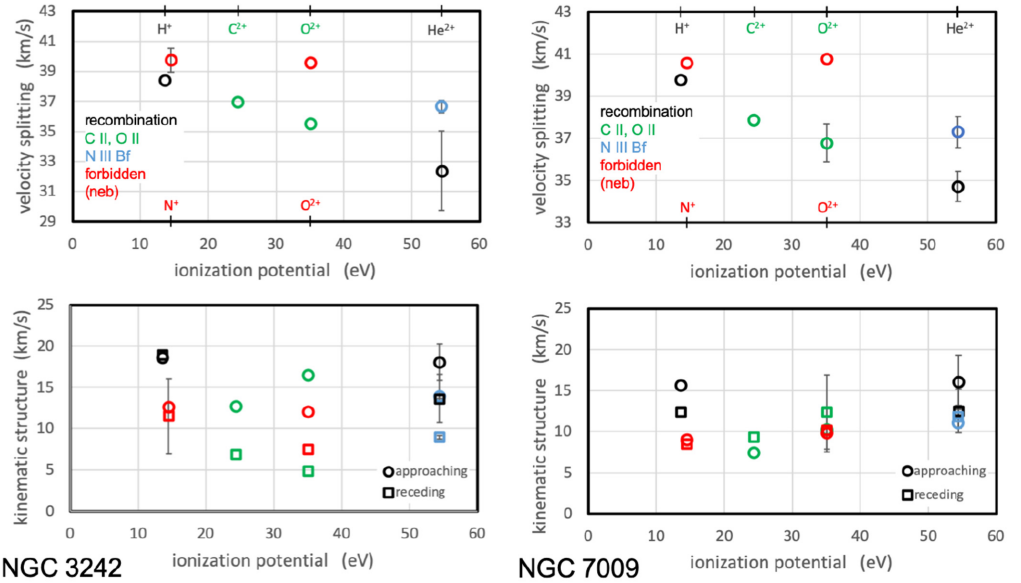

Figure 2. We present our results for NGC 3242 (left) and NGC 7009 (right) using the MES spectra. In the top panels, we present the usual "Wilson diagram" of velocity splitting plotted as a function of the ionization potential of the parent ion. The different colours indicate lines formed from different physical mechanisms. The bottom panels present the residual kinematic structure as a function of the ionization potential of the parent ion (shown, top/bottom axes). The circles and squares present the results for the approaching and receding sides, respectively. For NGC 3242, the velocity splitting varies from about 32 km/s for He II to 40 km/s for [N II], which means that the velocity gradient from the innermost part of the shell to the outermost part is of order 4 km/s. On the other hand, the residual kinematic structure is of order $10-15$ km/s, which is several times higher. The same situation occurs in NGC 7009: The velocity gradient is again of order 4 km/s while the residual kinematic structure is again aproximately three times larger, $10-15$ km/s.

we measure the FWHM of the arc lines closest to the wavelength of the line of interest since the spectral resolution of the MES spectra varies across the spectral intervals (at this very high resolution; $FWHM_{psf} = 3-5$ km/s).

For the UVES spectra of NGC 6153, the foregoing applies generally. However, the spectral resolution varies rather little, so we adopted a constant value of the instrumental broadening of $FWHM_{psf} = 11$ km/s.

Figures 2 and 3 present our results. The top panel for each object presents the "Wilson diagram" of velocity splitting as a function of the ionization potential of the parent ion of the line (Wilson 1950). For permitted lines, the parent ion is the ion that captures the electron whose emission cascade is observed, e.g., H^+ ions capture electrons, but we observe H I lines, so the relevant ionization potential is that to produce H^+. On the other hand, forbidden lines arise from the excitation of electrons already attached to the ions, e.g., [O III] λ5007 arises from the excitation of electrons attached to O^{2+} ions, so the relevant ionization potential is that to produce O^{2+}. The other case we observe are the Bowen fluorescence lines of N III whose ultimate origin is due to emission of He II Lyα photons, so the relevant ionization potential is that to produce He^{2+}.

From the Wilson diagrams, we can easily estimate the velocity gradient from the innermost to the outermost parts of nebular shell based upon the He II and [N II] lines. We estimate the velocity gradient as half the difference between the velocity splitting observed for the He II and [N II] lines. For example, in NGC 3242, the velocity splitting

https://doi.org/10.1017/S1743921324000462 Published online by Cambridge University Press

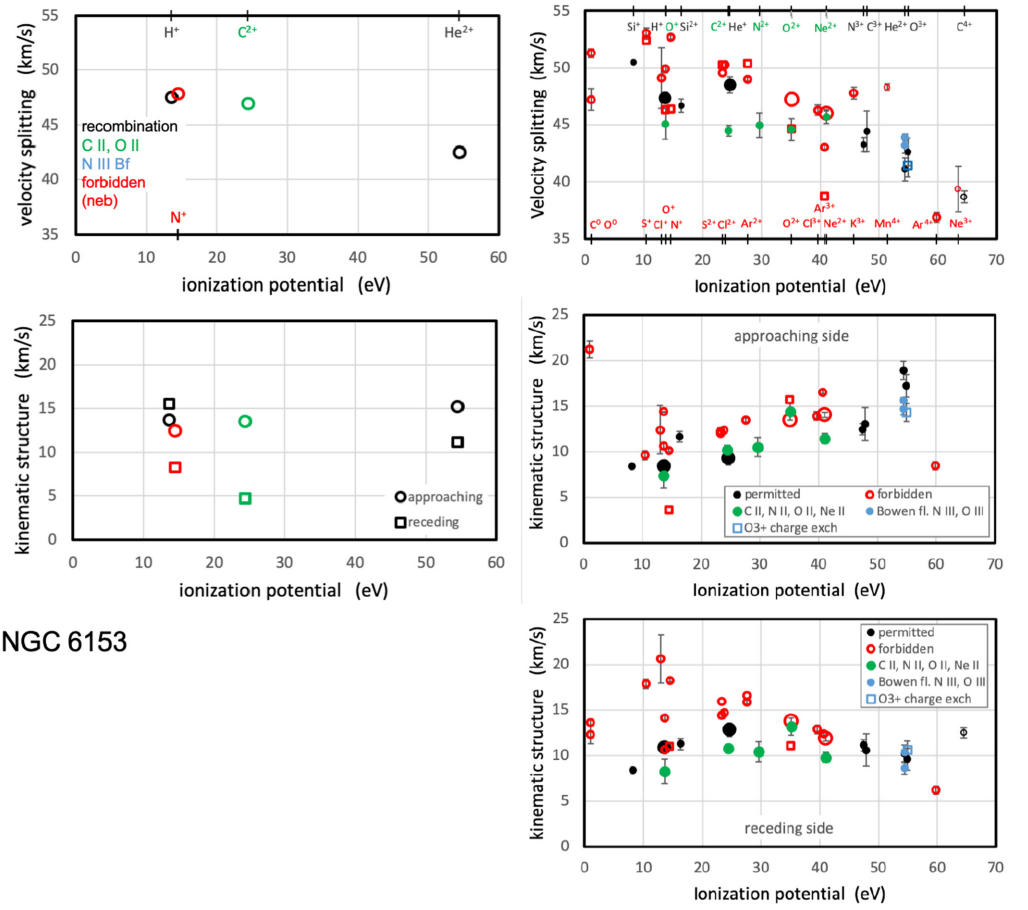

Figure 3. This figure presents our results for NGC 6153 using the MES spectra (left) and UVES spectra (right). Given the large number of lines measured in the UVES spectra, we present the kinematic structure for the approaching (middle panel) and receding (bottom) sides separately. The measurements are made along the line of sight to the central star for the MES spectra, but along a line of sight slightly offset from the central star (towards the ESE; Richer et al. 2022) for the UVES spectrum. Both datasets reveal results similar to NGC 3242 and NGC 7009: The velocity gradient through the nebular shell is $3-4$ km/s while the residual kinematic structure is aproximately three times larger, about 12 km/s.

is approximately 32 km/s for He II and 40 km/s for [N II], so the difference is 8 km/s. However, this velocity difference is measured over a line of sight that crosses both the approaching and receding sides of the nebular shell. Hence, the velocity gradient from the inner to outer edge of the nebular shell should be only about half of this value, or 4 km/s.

The bottom (or subsequent) panels in each column in Figures 2 and 3 present the residual kinematic structure, ΔW_{ks}, as a function of the ionization potential of the parent ion. Contrary to the velocity splitting, the kinematic structure does not vary in a systematic way with the ionization potential in these three objects. In some cases in Figures 2 and 3 there is a trend of ΔW_{ks} with ionization potential, but the sense of this trend is not systematic from one object to another. The most fundamental result from Figures 2 and 3 is that the residual kinematic structure is always substantially larger than the velocity gradient through the nebular shell, typically by a factor of 3 or more.

https://doi.org/10.1017/S1743921324000462 Published online by Cambridge University Press

4. Discussion

If we compare the residual kinematic structure we find in these three objects with the broadening mechanisms listed earlier, the residual kinematic structure is more important than any of them, except for thermal broadening of H and He lines. For the heavy elements C, N, and O, the residual kinematic structure is the dominant line broadening mechanism.

The fine structure of the H and He lines varies as a function of the electron temperature and density, but they are not a source of concern. The calculations of Clegg et al. (1999) indicate that temperature variations over the $300 - 30,000$ K range produce a change in the central wavelength of the blend by only 0.3 km/s for the H I lines. For He II λ4686, the effect is of 0.5 km/s for a temperature variation of $1,000 - 30,000$ K. Variations in the electron density have even less effect. So, this is not an important concern, as it is at least an order of magnitude smaller than the residual kinematic structure that we observe.

As we have defined it here, the residual kinematic structure includes all non-microscopic broadening mechanisms. One of these broadening mechanisms is the velocity gradient that is often observed through the nebular shell (Wilson 1950). This velocity gradient is well-understood from hydrodynamical models and arises because the innermost plasma cannot overrun the plasma that surrounds it (e.g., Villaver et al. 2002; Perinotto et al. 2004). The velocity gradient is a largely ordered velocity structure, so it's effect on broadening lines should be modest, except perhaps for lines like those of H that are emitted thoughout the entire nebular volume. However, we measure the velocity gradient directly here and find that it is always much less than the observed residual kinematic structure, with the two differing typically by a factor of 3 or more. Here, we consider only lines of sight toward or near the central star. These lines of sight are maximally sensitive to the effect of the velocity gradient, which only serves to emphasize that it is only a fraction of the residual kinematic structure. Hence, there is considerably more kinematic structure in nebular shells than the velocity gradient.

By considering the line of sight towards the central star (or very near it), we minimize the effects of projection along the line of sight (Sabbadin et al. 2008). This line of sight is radial through the nebular shell with respect to the central star. Other lines of sight will potentially intercept more structure, since they will traverse longer paths through nebular shell, if it is of constant thickness. However, as both the image and spectrum in Figure 1 clearly illustrate, the local structure is very variable and may well dominate over simple geometrical expectations.

Turbulence is likely the most obvious explanation for the residual kinematic structure we observe, as has been noted before (Sabbadin et al. 2008). Turbulence is also likely to have ample opportunity to be generated, since the small-scale structure (molecular) of planetary nebulae is notoriously non-uniform, even in highly evolved objects such as NGC 6720 or NGC 7293 where time might have been expected to allow the matter distribution to smooth itself out (Wesson et al. 2023; Su et al. 2007, respectively). This small-scale structure persists and must be continuously evaporated over the lifetime of the ionized shell and so provides many local sources of random velocity anomalies.

Whatever the origin of the residual kinematic structure, it is an energy source that contributes to the total energy budget. It would appear that it is also an important energy source, since the associated velocity, typically $10 - 15$ km/s here, is a large fraction of the thermal velocity of H atoms (21 km/s at 10^4 K). At face value, the energy associated with the residual kinematic structure may amount to of order 25% of the thermal energy, so this energy will affect the microphysics of the plasma. To our knowledge, this energy source has not been included thus far when modelling planetary nebulae.

https://doi.org/10.1017/S1743921324000462 Published online by Cambridge University Press

References

Clegg, R. E. S., Miller, S., Storey, P. J., & Kisielius, R. 1999, A&AS, 135, 359
Dekker, H., D'Odorico, S., Kaufer, A., Delabre, B., & Kotzlowski, H. 2000, Proc. SPIE, 4008, 534
García-Díaz, Ma. T., Henney, W. J., López, J. A., & Doi, T. 2008, RMxAA, 44, 181
Lang, K. R. 1980, Astrophysical Formulae (Berlin: Springer)
Massey, P., Valdes, F., & Barnes, J. 1992, IRAF User Guide 2B, A User's Guide to Reducing Slit Spectra with IRAF (Tucson, AZ: National Optical Astronomy Observatory)
Meaburn, J., López, J. A., Gutiérrez, L., et al. 2003, RMxAA, 39, 185
Perinotto, M., Schönberner, D., Steffen, M., & Calonaci, C. 2004, A&A, 414, 993
Pradhan, A. K., & Nahar, S. N. 2011, Atomic Astrophysics and Spectroscopy (Cambridge University Press)
Richer, M. G., Arrieta, A., Arias, L., et al. 2022, AJ, 164, 243
Richer, M. G., Suárez, G., López, J. A., & García-Díaz, Ma. T 2017, AJ, 153, 140
Sabbadin, F., Turatto, M., Benedetti, S., Ragazzoni, R., & Cappellaro, E. 2008, A&A, 488, 225
Su, K. Y., Chu, Y.-H., Rieke, G. H., et al. 2007, ApJL, 657, 41
Villaver, E., García-Segura, G., & Manchado, A. 2002, ApJ, 581, 1204
Wesson, R., Matsuura, M., Zijlstra, A. A., et al. 2023, arXiv:2308.09027
Wilson, O. C. 1950, ApJ, 111, 279

https://doi.org/10.1017/S1743921324000462 Published online by Cambridge University Press